British Journal of Cancer www.nature.com/bjc

ARTICLE

Molecular Diagnostics

Machine learning-based pathomics signature could act as a novel prognostic marker for patients with clear cell renal cell carcinoma

Siteng Chen[1,4], Liren Jiang[2,4], Feng Gao[2,4], Encheng Zhang[1], Tao Wang[1], Ning Zhang[3✉], Xiang Wang[1✉] and Junhua Zheng[1✉]

BACKGROUND: Traditional histopathology performed by pathologists through naked eyes is insufficient for accurate survival prediction of clear cell renal cell carcinoma (ccRCC).
METHODS: A total of 483 whole slide images (WSIs) data from three patient cohorts were retrospectively analyzed. We performed machine learning algorithm to identify optimal digital pathological features and constructed machine learning-based pathomics signature (MLPS) for ccRCC patients. Prognostic performance of the prognostic model was also verified in two independent validation cohorts.
RESULTS: MLPS could significantly distinguish ccRCC patients with high survival risk, with hazard ratio of 15.05, 4.49 and 1.65 in three independent cohorts, respectively. Cox regression analysis revealed that the MLPS could act as an independent prognostic factor for ccRCC patients. Integration nomogram based on MLPS, tumour stage system and tumour grade system improved the current survival prediction accuracy for ccRCC patients, with area under curve value of 89.5%, 90.0%, 88.5% and 85.9% for 1-, 3-, 5- and 10-year disease-free survival prediction.
DISCUSSION: The machine learning-based pathomics signature could act as a novel prognostic marker for patients with ccRCC. Nevertheless, prospective studies with multicentric patient cohorts are still needed for further verifications.

British Journal of Cancer (2022) 126:771–777; https://doi.org/10.1038/s41416-021-01640-2

BACKGROUND

Renal cancer is the sixth most common malignancy among males in the United States in 2021 [1]. Among multiple types of renal cancers, clear cell renal cell carcinoma (ccRCC) accounts for most of the cases [2]. The prognosis of ccRCC patients varies among different stages and some patients with poor stage tumour suffer from showed lower cure rate even after radical nephrectomy [3, 4]. TNM classifications, the most classical prognostic parameters, still have limitations as patients with the same TNM staging could show diverse clinical outcomes [5, 6]. Furthermore, International Society of Urological Pathology (ISUP) grading system mainly targets on histological nuclear morphology [4, 7]. Therefore, a more comprehensive prognosis prediction could be an intriguing topic.

Thanks to the novel high-throughput technology, artificial intelligence on histological characteristic recognition shows huge potential in clinical outcome prediction [8, 9]. Through comprehensive analysis of histological morphology, computational pathology is widely applied in diagnosis and survival prediction of various malignancies [10–14]. However, most of these studies are targeting on traditional optical microscopes, which may cause the narrow field of view problems compared with whole slide imaging (WSI), which could show both the tissue and cell structures of tumour tissue at different magnification [15].

Here, in this study, we constructed a machine learning-based pathomics signature (MLPS) from WSIs to analyze and predict the clinical outcomes of ccRCC patients, which might provide intelligent advice for clinicians to facilitate the process of individualised treatment.

METHODS

Patient cohorts and data resource

Patient cohorts recruited in this study come from three independent data source—Clinical Proteomic Tumor Analysis Consortium (CPTAC cohort); Shanghai General Hospital (General cohort) and The Cancer Genome Atlas (TCGA cohort). We recruited 146 ccRCC patients from Shanghai General Hospital, who underwent radical or partial nephrectomy from January 2012 to December 2018. All of the included patients shall meet the following the inclusion criteria: (i) pathologically diagnosed as ccRCC without other types of malignant tumours; (ii) with unabridged clinical and pathologic information and disease-free survival (DFS) follow-up data; (iii) with access to corresponding tumour samples. DFS was defined as the time from

[1]Department of Urology, Shanghai General Hospital, Shanghai Jiao Tong University School of Medicine, Shanghai, China. [2]Department of Pathology, Shanghai General Hospital, Shanghai Jiao Tong University School of Medicine, Shanghai, China. [3]Department of Urology, Ruijin Hospital, Shanghai Jiao Tong University School of Medicine, Shanghai, China. [4]These authors contributed equally: Siteng Chen, Liren Jiang, Feng Gao. ✉email: zn12235@rjh.com.cn; xiang.wang1@shgh.cn; zhengjh0471@sjtu.edu.cn

Received: 5 May 2021 Revised: 26 October 2021 Accepted: 10 November 2021
Published online: 25 November 2021

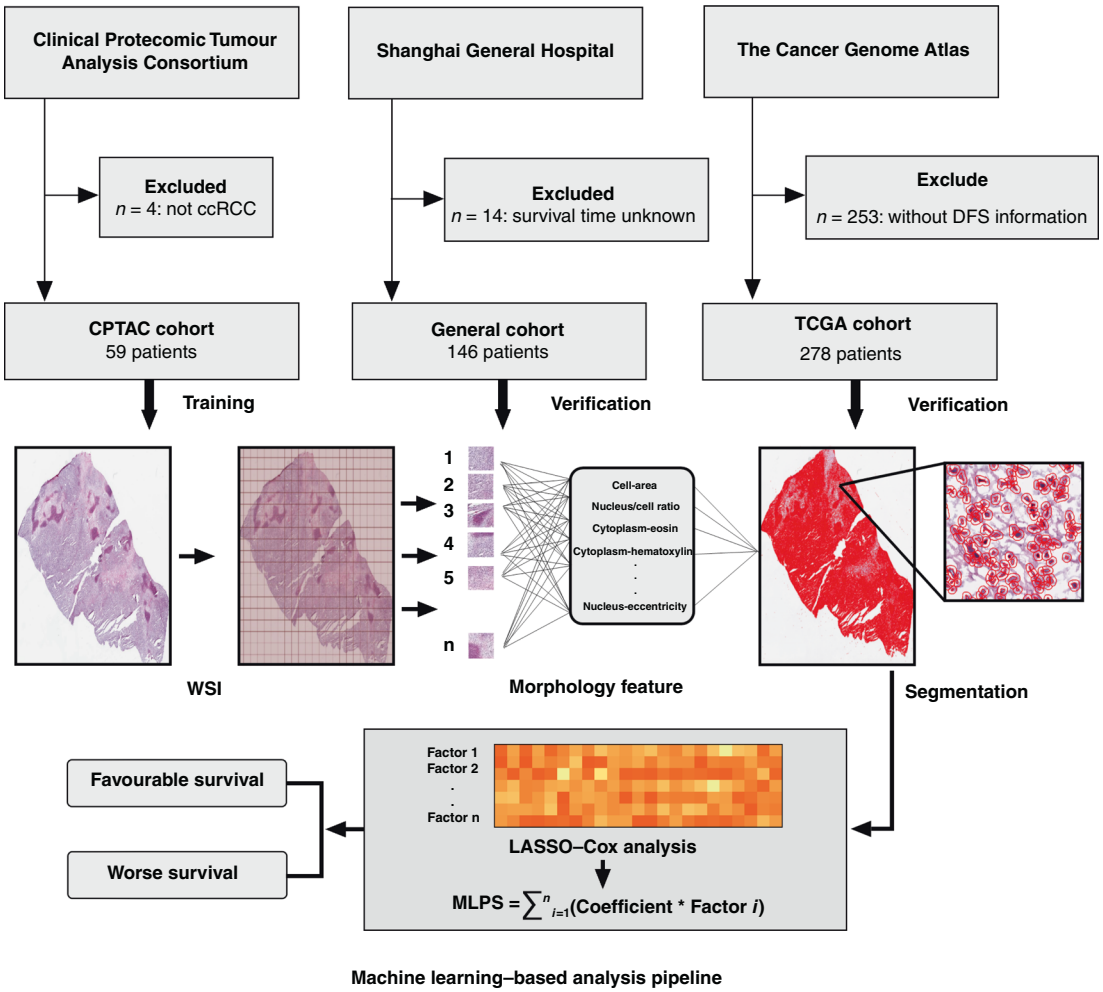

Fig. 1 The workflow of histopathology image processing and machine learning analysis in this study. WSI whole slide image.

primary surgery to first tumour recurrence, progression, death or last follow-up for censoring patients. Tumour samples were paraffin-embedded and sectioned to make formalin-fixed and paraffin-embedding (FFPE) sections for further Hematoxylin-eosin (H&E) staining. Ethical approval of our study has been approved from the Research Ethics Committee of Shanghai General Hospital.

A total of 59 ccRCC patients with access to histopathology H&E images and DFS follow-up information were acquired from CPTAC database (https://proteomics.cancer.gov/programs/cptac) database and the Cancer Imaging Archive [16], which abided by the Creative Commons Attribution 3.0 Unported License. Another 278 ccRCC patients meeting the first two criteria mentioned above and with open-access to histopathology H&E images from TCGA were also enrolled in this study. Original H&E images and detailed clinical information, including the DFS follow-up data, was downloaded from the TCGA database (https://portal.gdc.cancer.gov/).

Hematoxylin-eosin staining

FFPE sections were first stained with hematoxylin (Sigma–Aldrich) and 1% acid ethanol (Sigma–Aldrich), which were rinsed in distilled water. Secondly, the sections were stained by eosin (Sigma–Aldrich) for 3 min and further dehydrated with graded alcohol. All of the H&E-stained sections were scanned through Leica Aperio AT2 (Leica Biosystems Inc., Frankfurt, Germany) for WSI.

Whole slide image process and analysis pipeline

WSIs of H&E staining slides without any preprocessing were firstly segmented into tiles, and then imported and detected in QuPath digital pathology software [17] to carrying out cell and nuclear segmentation. By applying the cell detection function from the analysis module, the nuclear segmentation was performed to recognise objects through Watershed cell detection based on segmentation parameters [18], including morphology features of cell, nuclear, and cytoplasm. The setup parameter was set as hematoxylin OD for detection image, with pixel size of 0.5 µm. For nucleus parameters, the background radius and sigma were set as 8 and 1.5 µm, respectively. For intensity parameters, the threshold was set as 0.1 and the max background intensity was set as 2. Other parameters were set as their respective default values. Smooth boundaries and parameter measurements were also applied in the process of WSIs. Subsequently, a total of 43 different pathological signatures were detected and measured for every recognised object in each segmented tile (Table S1).

An analysis pipeline was constructed to analyze the detected H&E image features for different clinical applications in the training cohort (CPTAC cohort). We performed least absolute shrinkage and selection operator via *glmnet* package [19] to identify optimal digital pathological features and calculate coefficients of each features in the model of MLPS. For the MLPS, the tenfold cross-validated error and varying-level penalisation progress were shown in Figs. S1 and S2. The workflow of histopathology image processing and analysis pipeline was shown in Fig. 1.

Statistical analysis

In this study, R 3.6.2 were used to conduct the data analysis and visualisation. Kaplan–Meier (KM) curve analysis with hazard ratio (HR) and 95% confidence interval (CI) were carried out via log-rank test to find out different clinical outcomes. Univariate and multivariate Cox regression analysis were carried out to identify prognostic markers for patients with ccRCC. The specificity and sensitivity of the prediction model were evaluated through receiver operating characteristic (ROC) curve with area under the curve (AUC) value.

Table 1. Basic clinical characteristics of patients from three independent patient cohorts.

	CPTAC cohort (59)	General cohort (146)	TCGA cohort (278)
Age (years)			
≥65	28 (47.5%)	45 (30.8%)	93 (33.5%)
<65	31 (52.5%)	101 (69.2%)	185 (66.5%)
Sex			
Male	37 (62.7%)	115 (78.8%)	182 (65.5%)
Female	22 (37.3%)	31 (21.2%)	96 (34.5%)
Grade			
G1	3 (5.1%)	14 (9.6%)	7 (2.5%)
G2	37 (62.7%)	79 (54.1%)	119 (42.8%)
G3	15 (25.4%)	48 (32.9%)	116 (41.7%)
G4	4 (6.8%)	5 (3.4%)	36 (13.0%)
Stage			
i	30 (50.8%)	128 (87.6%)	134 (48.2%)
ii	6 (10.2%)	9 (6.2%)	29 (10.4%)
iii	18 (30.5%)	9 (6.2%)	73 (26.3%)
iv	5 (8.5%)	0	42 (15.1%)
T stage			
T1	32 (54.2%)	128 (87.6%)	137 (49.3%)
T2	7 (11.9%)	9 (6.2%)	36 (12.9%)
T3	19 (32.2%)	9 (6.2%)	103 (37.1%)
T4	1 (1.7%)	0	2 (0.7%)
N stage			
N1	/	2 (1.4%)	8 (2.9%)
N0	/	14 4(98.6%)	270 (97.1%)
M stage			
M1	/	0	41 (14.7%)
M0	/	146 (100%)	237 (85.3%)
DFS status			
Yes	45 (76.3%)	131 (89.7%)	185 (66.5%)
No	14 (23.7%)	15 (10.3%)	93 (33.5%)

CPTAC Clinical Proteomic Tumor Analysis Consortium, *TCGA* The Cancer Genome Atlas, *DFS* disease-free survival.

RESULTS

Clinical and pathological characteristics

The clinical and pathological features of the CPTAC cohort ($n = 59$), the General cohort ($n = 146$) and the TCGA ($n = 278$) cohort were shown in Table 1, with mean follow-up duration of 26.4 ± 16.8, 54.9 ± 27.8 and 43.2 ± 30.6 months, respectively. Male patients took up larger proportion than female in all the three cohorts (62.7%, 78.8% and 65.5%). A greater number of patients with G2/G3 tumour were also observed in the three cohorts (88.1%, 87.0% and 84.5%). While patients with lymphatic metastasis or distant metastasis were rarely seen in these cohorts.

Prognostic image factors in LASSO analysis and the development of the MLPS classification system

As shown in Fig. S1, the left vertical line which equaled to the minimum tenfold cross-validated error arrived at 5, indicating that five image factors were screened out to be the most prognostic factors for patients with ccRCC. The selected image factors included Nucleus Circularity, Nucleus Min caliper, Nucleus Hematoxylin OD mean, Nucleus Hematoxylin OD min and Cell Eosin OD std dev.

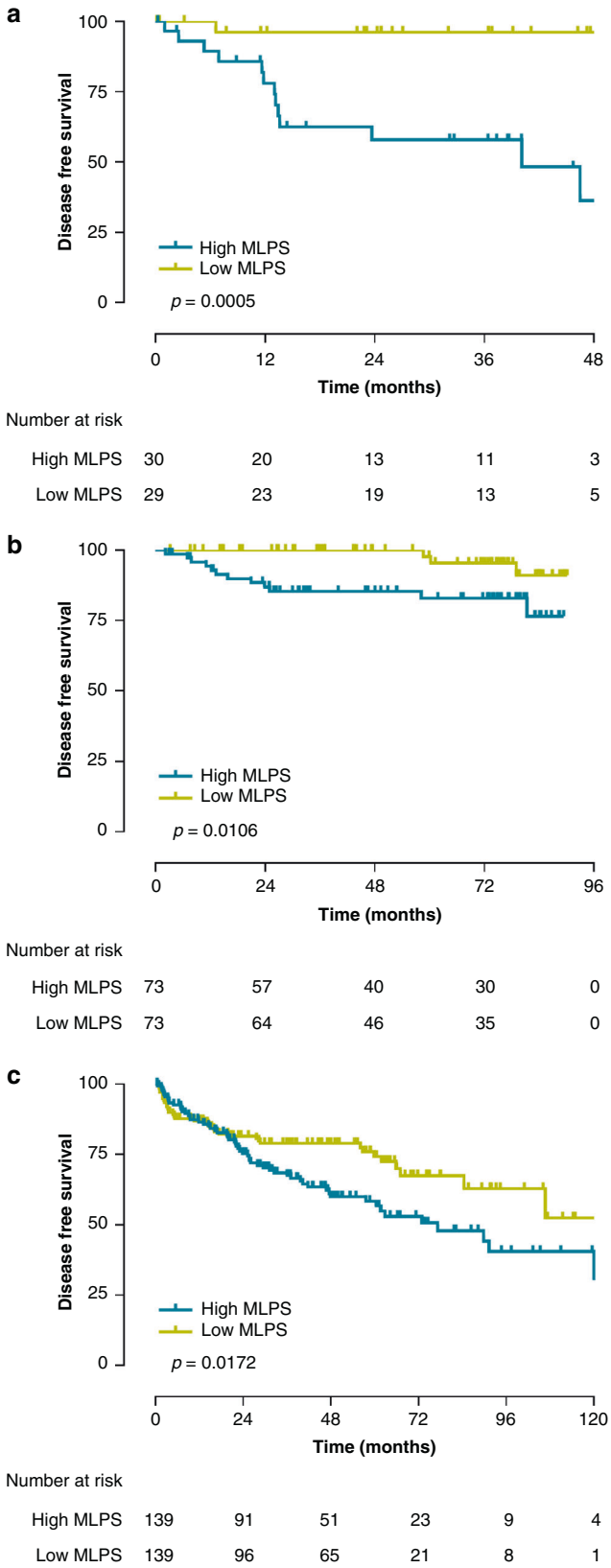

Fig. 2 Kaplan–Meier survival analysis of disease-free survival predicted by MLPS for ccRCC patients. a The CPTAC cohort; **b** The General cohort; **c** The TCGA cohort. ccRCC clear cell renal cell carcinoma, MLPS machine learning-based pathomics signature, CPTAC Clinical Proteomic Tumor Analysis Consortium, TCGA The Cancer Genome Atlas.

Table 2. Univariate and multivariate cox regression analysis of prognostic markers three independent patient cohorts.

		Univariate		Multivariate	
		HR (95% CI)	***p***	**HR (95% CI)**	***p***
CPTAC cohort	Grade				
	G3/4 vs G1/2	1.68 (0.58–4.85)	0.337	/	/
	Stage				
	iii/iv vs i/ii	9.94 (2.22–44.52)	**0.003**	6.75 (1.49–30.62)	**0.013**
	Sex				
	Male vs female	0.81 (0.27–2.43)	0.711	/	/
	Age				
	≥65 vs <65	0.64 (0.21–1.90)	0.419	/	/
	MLPS				
	High vs low	15.28 (2.00–117.05)	**0.009**	10.20 (1.32–79.05)	**0.026**
General cohort	Grade				
	G3/4 vs G1/2	11.15 (3.04–40.92)	**<0.0001**	5.83 (1.43–23.76)	**0.014**
	Stage				
	ii/iii vs i	7.90 (2.85–21.87)	**<0.0001**	6.16 (1.84–20.67)	**0.003**
	Sex				
	Male vs female	29.28 (0.15–>100)	0.211	/	/
	Age				
	≥65 vs <65	2.79 (1.01–7.74)	**0.048**	4.10 (1.18–14.23)	**0.026**
	MLPS				
	High vs low	4.5 (1.27–15.97)	**0.02**	9.73 (2.16–43.78)	**0.003**
TCGA cohort	Grade				
	G3/4 vs G1/2	3.11 (1.92–5.02)	**<0.0001**	1.99 (1.21–3.27)	**0.007**
	Stage				
	iii/iv vs i/ii	5.82 (3.63–9.33)	**<0.0001**	4.92 (3.02–8.04)	**<0.0001**
	Sex				
	Male vs female	1.29 (0.83–2.00)	0.261	/	/
	Age				
	≥65 vs <65	1.10 (0.72–1.69)	0.656	/	/
	MLPS				
	High vs low	1.65 (1.09–2.51)	**0.018**	1.78 (1.17–2.71)	**0.007**

HR hazard ratio, *CI* confidence interval, *CPTAC* Clinical Proteomic Tumor Analysis Consortium, *MLPS* machine learning-based pathomics signature, *TCGA* The Cancer Genome Atlas, *DFS* disease-free survival.
Bold values indicate statistical significance $p < 0.05$.

The regression coefficients (β) of each selected image factors were also extracted from the LASSO analysis in Fig. S2 ($\beta_{\text{Nucleus Circularity}} = -23.8919605$, $\beta_{\text{Nucleus Min caliper}} = -0.6106737$, $\beta_{\text{Nucleus Hematoxylin OD mean}} = -1.7673163$, $\beta_{\text{Nucleus Hematoxylin OD min}} = -2.1720564$, $\beta_{\text{Cell Eosin OD std dev}} = -7.2948452$). The formula MLPS was then established as follows: MLPS = Nucleus Circularity*(−23.8919605) + Nucleus Min caliper*(−0.6106737) + Nucleus Hematoxylin OD mean*(−1.7673163) + Nucleus Hematoxylin OD min*(−2.1720564) + Cell Eosin OD std dev*(−7.2948452).

Survival analysis and Cox regression analysis based on the MLPS classification in independent patient cohorts

The cut-off value of MLPS was set up as the median value of each patient cohort, and patients in each cohort were grouped into high or low MLPS group. The KM survival curve for the CPTAC cohort stratified into high or low MLPS were plotted in Fig. 2a. Patients in high MLPS subgroup exhibited significantly worse clinical prognosis when compared with patients with low MLPS (HR = 15.05, 95% CI: 5.27–43.04, $p = 0.0005$). Verification of KM survival curve analyses were further performed in the General and TCGA cohorts. The MLPS classification system was able to distinguish patients associated with worse DFS in both the two independent cohorts, with HR of 4.49 (95% CI: 1.63–12.38, $p = 0.0106$) in the General cohort (Fig. 2b) and 1.65 (95% CI: 1.10–2.48, $p = 0.0172$) in the TCGA cohort (Fig. 2c).

Results from Cox regression analysis were illustrated in Table 2. In the CPTAC cohort, the tumour staging system and the MLPS classification system were the independent prognostic factors for DFS of ccRCC patients. In the General cohort, the tumour staging system, the tumour grading system, patient age and the MLPS classification system were proved to be independently associated with DFS of patients with ccRCC. While in the TCGA cohort, the tumour staging system, the tumour grading system and the MLPS classification system were found to be the independent prognostic factors. HR of the MLPS classification system was observed to be larger than others in the CPTAC and TCGA cohorts.

Integration nomogram improves the current survival prediction accuracy for ccRCC patients

To improve current survival prediction accuracy for ccRCC patients, an integration nomogram was established based on the MLPS classification system and predictable clinical and

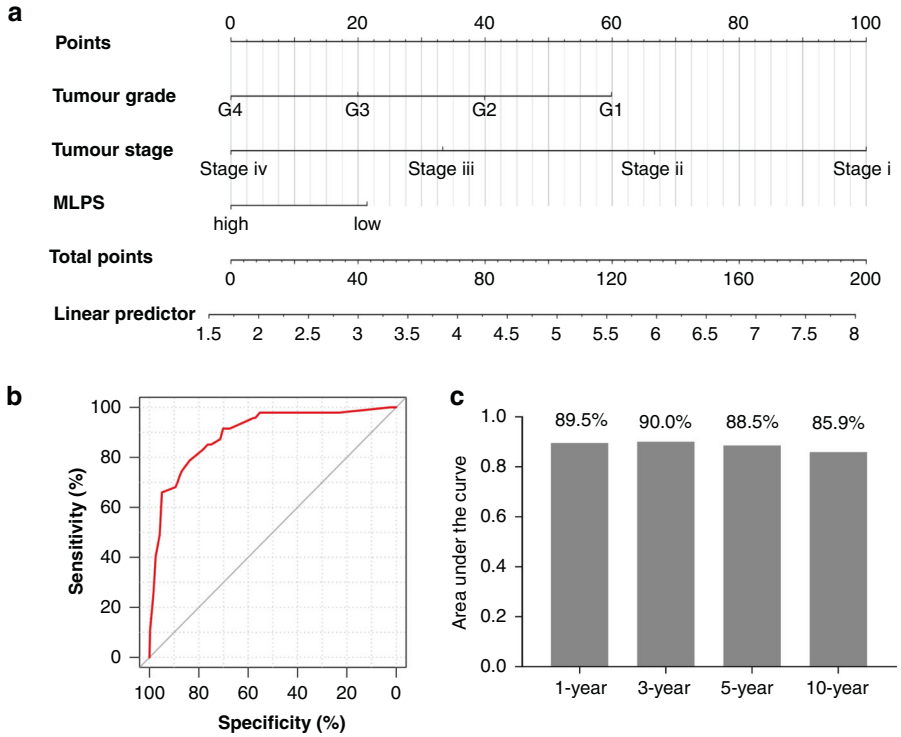

Fig. 3 Developed and evaluated a prognostic nomogram in the whole patient cohort. a Nomogram based on MLPS and clinicopathologic factors for disease-free survival prediction of ccRCC patients. **b** ROC analysis for evaluating 1-year disease-free survival prediction of the nomogram in the whole patient cohort. **c** Area under the curve from ROC analysis for evaluating 1-, 3-, 5- and 10-year disease-free survival prediction of the nomogram. ccRCC clear cell renal cell carcinoma, ROC receiver operating characteristic, MLPS machine learning-based pathomics signature.

Table 3. Receiver operating characteristic curve analysis for evaluating the accuracy of prognostic model in three independent patient cohorts.

		AUC	95% CI	*p*
CPTAC cohort	1 year	0.952	0.862–0.991	<0.0001
	3 year	0.941	0.848–0.986	<0.0001
	5 year	0.864	0.750–0.940	<0.0001
	10 year	0.864	0.750–0.940	<0.0001
General cohort	1 year	0.896	0.835–0.940	<0.0001
	3 year	0.923	0.867–0.960	<0.0001
	5 year	0.898	0.837–0.942	<0.0001
	10 year	0.814	0.741–0.874	<0.0001
TCGA cohort	1 year	0.871	0.826–0.908	<0.0001
	3 year	0.878	0.833–0.914	<0.0001
	5 year	0.877	0.833–0.913	<0.0001
	10 year	0.853	0.806–0.892	<0.0001

AUC area under curve, *CI* confidence interval, *CPTAC* Clinical Proteomic Tumor Analysis Consortium, *TCGA* The Cancer Genome Atlas.

pathological factors (Fig. 3a) in the whole patient cohort. ROC curve analyses indicated that AUC values for 1-, 3-, 5- and 10-year DFS prediction arrived at 89.5%, 90.0%, 88.5% and 85.9%, respectively, revealing the wonderful performance of the integration nomogram (Fig. 3b, c). Further subgroup analysis also revealed the high accuracy of prognostic prediction of the prognostic nomogram in these three independent patient cohorts for ccRCC patients (Table 3).

DISCUSSION

Traditional microscopic views of pathological images can be distinguished by the cellular structures, especially the important nuclear structures. However, tissue structures, such as tumour infiltrations in surrounded mesenchymal cells, are missing. WSIs contain multiple histological features, including not only cellular information but also tissue arrangement [15]. In addition, WSIs could reflect the pT stages of ccRCC based on the tumour infiltration in depth and ranges, reflecting better prognostic values. Hence, the integrate pathological features on WSI suggest its incomparable advantage over traditional microscopic views of images.

The advent of artificial intelligence technology has deeply affected the traditional pathological diagnosis and prognosis prediction [20, 21]. With the uprising application of WSIs, automated histological analysis among multiple cancers showed its promising blueprints in both diagnosis and clinical outcome prediction [22, 23]. Furthermore, through integrated information of WSIs, pathomics greatly improves the performance of computational pathology [15]. However, studies on computational pathology with WSIs in ccRCC is rarely reported for now.

In this study, through the application of WSIs, we constructed a machine learning-based prognosis model for survival predicting of ccRCC patients. The MLPS showed high predicting accuracy among three independent patient cohorts. Among different time scales, 1-year and 3-year disease-free survival prediction showed highest accuracy. Results from Cox regression analysis were illustrated that the MLPS could act as an independent prognostic factor for DFS of ccRCC patients. Integration nomogram, which combined the MLPS and clinicopathologic factors, improves the current survival prediction accuracy with AUC values for 1-, 3-, 5- and 10-year DFS prediction arrived at 89.5%, 90.0%, 88.5% and 85.9%, respectively, revealing the wonderful performance of the integration nomogram.

The selected image factors, including Nucleus Circularity, Nucleus Min caliper, Nucleus Hematoxylin OD mean, Nucleus Hematoxylin OD min and Cell Eosin OD std dev, were mainly related to the shape and staining depth of cell nuclear, reflecting the close connection between nuclear heteromorphism of cancer cell and clinical prognosis. Therefore, our machine learning-based prediction model might investigate the histopathology appearance of cell nuclear and distinguish the features that were significantly associated with poor clinical outcomes of patients with ccRCC.

TNM classifications, as the most classical prognosis evaluation system, have been applied to predict the survival and assist the treatment design for all the cancer patients [5, 24]. The criteria of TNM staging are mainly regarding the macroscopic features. However, different pathological diagnosis within the same organ may also show different prognosis, for instance high-grade ccRCC and high-grade collecting duct carcinoma both belong to renal cell tumours but with different prognosis [2]. Even the same grade of ccRCC patients could show diverse prognosis because of the cellular difference [2, 5, 24].

Additionally, based on the nuclear abnormality of ccRCC, ISUP grading system proves its value in survival predicting for ccRCC patients [4]. Higher grades are associated with worse clinical outcomes [4]. Nevertheless, ISUP grading system does not evaluate macroscopic features. During clinical practice, clinicians usually combine TNM and ISUP classifications for better treatment decision. Here in this study, the application of WSIs and combination of clinicopathologic factors can help clinicians with better visualised survival prediction.

There are some limitations in this study. First, the cut-off values of MLPS were set up as the median values among three cohorts, which were not fixed values. Furthermore, even though our prediction model performed well in distinguishing patients with high survival risk, the study was retrospective and need further prospective validations for the application of this system into clinical practice. Additionally, considering different H&E staining protocols among different patient cohorts, WSIs may show somewhat colour heterogeneity, which might affect the analysis.

CONCLUSION

In conclusion, in this study, we developed and verified a pathomics signature based on machine learning methods from WSIs. The MLPS could act as an excellent survival predictor for ccRCC patients, which could help to aid clinical decision making. Nevertheless, prospective studies with multicentric patient cohorts are still needed for further verifications.

DATA AVAILABILITY

Data supporting the findings of this study are available within the supplementary information and are also available from the authors upon reasonable request.

CODE AVAILABILITY

The code used for slide image process and feature extraction had been made publicly available at https://qupath.github.io/ [17].

REFERENCES

1. Siegel RL, Miller KD, Fuchs HE, Jemal A. Cancer statistics, 2021. CA Cancer J Clin. 2021;71:7–33.
2. Humphrey PA, Moch H, Cubilla AL, Ulbright TM, Reuter VE. The 2016 WHO classification of tumours of the urinary system and male genital organs-Part B: prostate and bladder tumours. Eur Urol. 2016;70:106–19.
3. Liu L, Qi L, Li Y, Chen M, Li C, Cheng X, et al. Retroperitoneoscopic partial nephrectomy for moderately complex ventral hilar tumors: surgical technique and trifecta outcomes from a single institution in China. J Laparoendosc Adv Surg Tech Part A. 2017;27:812–7.
4. Yi X, Xiao Q, Zeng F, Yin H, Li Z, Qian C, et al. Computed tomography radiomics for predicting pathological grade of renal cell carcinoma. Front Oncol. 2020;10:570396.
5. Inamura K, Fujiwara T, Hoshida Y, Isagawa T, Jones MH, Virtanen C, et al. Two subclasses of lung squamous cell carcinoma with different gene expression profiles and prognosis identified by hierarchical clustering and non-negative matrix factorization. Oncogene. 2005;24:7105–13.
6. Chen ST, Zhang N, Jiang LR, Gao F, Shao JL, Wang T, et al. Clinical use of a machine learning histopathological image signature in diagnosis and survival prediction of clear cell renal cell carcinoma. Int J Cancer. 2021;148:780–90.
7. Delahunt B, Cheville JC, Martignoni G, Humphrey PA, Magi-Galluzzi C, McKenney J, et al. The International Society of Urological Pathology (ISUP) grading system for renal cell carcinoma and other prognostic parameters. Am J Surg Pathol. 2013;37:1490–504.
8. Klimov S, Miligy IM, Gertych A, Jiang Y, Toss MS, Rida P, et al. A whole slide image-based machine learning approach to predict ductal carcinoma in situ (DCIS) recurrence risk. Breast Cancer Res. 2019;21:83.
9. Louis DN, Gerber GK, Baron JM, Bry L, Dighe AS, Getz G, et al. Computational pathology: an emerging definition. Arch Pathol Lab Med. 2014;138:1133–8.
10. Gertych A, Ing N, Ma Z, Fuchs TJ, Salman S, Mohanty S, et al. Machine learning approaches to analyze histological images of tissues from radical prostatectomies. Comput Med Imaging Graph. 2015;46:197–208.
11. Ehteshami Bejnordi B, Veta M, Johannes van Diest P, van Ginneken B, Karssemeijer N, Litjens G, et al. Diagnostic assessment of deep learning algorithms for detection of lymph node metastases in women with breast cancer. JAMA. 2017;318:2199–210.
12. Yu KH, Zhang C, Berry GJ, Altman RB, Re C, Rubin DL, et al. Predicting non-small cell lung cancer prognosis by fully automated microscopic pathology image features. Nat Commun. 2016;7:12474.
13. Kickingereder P, Isensee F, Tursunova I, Petersen J, Neuberger U, Bonekamp D, et al. Automated quantitative tumour response assessment of MRI in neuro-oncology with artificial neural networks: a multicentre, retrospective study. Lancet Oncol. 2019;20:728–40.
14. Brinker TJ, Hekler A, Enk AH, Berking C, Haferkamp S, Hauschild A, et al. Deep neural networks are superior to dermatologists in melanoma image classification. Eur J Cancer. 2019;119:11–7.
15. Cao R, Yang F, Ma SC, Liu L, Zhao Y, Li Y, et al. Development and interpretation of a pathomics-based model for the prediction of microsatellite instability in Colorectal Cancer. Theranostics. 2020;10:11080–91.
16. Clark K, Vendt B, Smith K, Freymann J, Kirby J, Koppel P, et al. The Cancer Imaging Archive (TCIA): maintaining and operating a public information repository. J Digit Imaging. 2013;26:1045–57.
17. Bankhead P, Loughrey MB, Fernández JA, Dombrowski Y, McArt DG, Dunne PD, et al. QuPath: Open source software for digital pathology image analysis. Sci Rep. 2017;7:16878.
18. Kulkarni PM, Robinson EJ, Sarin Pradhan J, Gartrell-Corrado RD, Rohr BR, Trager MH, et al. Deep learning based on standard H&E images of primary melanoma tumors identifies patients at risk for visceral recurrence and death. Clin Cancer Res. 2020;26:1126–34.
19. Friedman J, Hastie T, Tibshirani R. Regularization paths for generalized linear models via coordinate descent. J Stat Softw. 2010;33:1–22.
20. Schuettfort VM, Pradere B, Rink M, Comperat E, Shariat SF. Pathomics in urology. Curr Opin Urol. 2020;30:823–31.
21. Jiang Y, Jin C, Yu H, Wu J, Chen C, Yuan Q, et al. Development and validation of a deep learning CT signature to predict survival and chemotherapy benefit in gastric cancer: a multicenter, retrospective study. Ann Surg. 2021;274:e1153–61.
22. Esteva A, Kuprel B, Novoa RA, Ko J, Swetter SM, Blau HM, et al. Dermatologist-level classification of skin cancer with deep neural networks. Nature. 2017;542:115–8.
23. Zhao K, Li Z, Yao S, Wang Y, Wu X, Xu Z, et al. Artificial intelligence quantified tumour-stroma ratio is an independent predictor for overall survival in resectable colorectal cancer. EBioMedicine. 2020;61:103054.
24. Beer DG, Kardia SL, Huang CC, Giordano TJ, Levin AM, Misek DE, et al. Gene-expression profiles predict survival of patients with lung adenocarcinoma. Nat Med. 2002;8:816–24.

ACKNOWLEDGEMENTS

We appreciate the QuPath digital pathology software for its contribution. Open data used in this publication were generated by the National Cancer Institute Clinical Proteomic Tumor Analysis Consortium (CPTAC) and TCGA database.

AUTHOR CONTRIBUTIONS

NZ, XW, JZ and SC participated in the study conception and design, data collection, data analysis, reviewed the paper and approved the final draft for submission. LJ, FG, EZ and TW participated in data collection, reviewed the paper and approved the final draft for submission.

FUNDING INFORMATION

This work was supported by the National Natural Science Foundation of China (81972393 and 82002665). The funding sources had no role in the design of the study; collection, analysis or interpretation of the data; writing of the report; the decision to submit for publication.

ETHICS APPROVAL AND CONSENT TO PARTICIPATE

The ethical approval of this study has been approved from the Research Ethics Committee of Shanghai General Hospital (approval number: 2021SQ121). Not further ethical approval was required since all the slice images from the CPTAC cohort and the TCGA cohort were publicly available for research purposes.

CONSENT TO PUBLISH

Not applicable.

COMPETING INTERESTS

The authors declare no competing interests.

ADDITIONAL INFORMATION

Supplementary information The online version contains supplementary material available at https://doi.org/10.1038/s41416-021-01640-2.

Correspondence and requests for materials should be addressed to Ning Zhang, Xiang Wang or Junhua Zheng.